



New single-source precursor for bismuth sulfide and its use as low-cost counter electrode material for dye-sensitized solar cells



Ratna Chauhan^a, Jyotsna Chaturvedi^b, Manoj Trivedi^c, Jyoti Singh^d, Kieran C. Molloy^{e,*}, Gabriele Kociok-Köhn^e, Dinesh P. Amalnerkar^a, Abhinav Kumar^{f,*}

^a Center for Materials for Electronic Technology, Panchwati, Pune, India

^b Department of Physical and Inorganic Chemistry, Indian Institute of Science, Bangalore, India

^c Department of Chemistry, University of Delhi, Delhi 110 007, India

^d Department of Chemistry, Deen Dayal Upadhyaya College, University of Delhi, India

^e Department of Chemistry, University of Bath, Bath BA2 7AY, UK

^f Department of Chemistry, University of Lucknow, Lucknow 226 007, India

ARTICLE INFO

Article history:

Received 11 January 2015

Received in revised form 9 March 2015

Accepted 11 March 2015

Available online 18 March 2015

Keywords:

Bi₂S₃

X-ray crystallography

TGA-DTA

Counter electrode

DSSC

ABSTRACT

One new homoleptic [Bi(dtc)₃] (**1**) (dtc = 4-hydroxypiperidine dithiocarbamate) has been synthesized and characterized by microanalysis, IR, UV-Vis, ¹H and ¹³C spectroscopy and X-ray crystallography. The photoluminescence spectrum for the compound in DMSO solution was recorded. The crystal structure of **1** displayed distorted octahedral geometry around the Bi(III) center bonded through sulfur atoms of the dithiocarbamate ligands. TGA indicates that the compound decomposes to a Bi and Bi-S phase system. The Bi and Bi-S obtained from decomposition of the compound have been characterized by pXRD, EDAX and SEM. Solvothermal decomposition of **1** in the absence and presence of two different capping agents yielded three morphologically different Bi₂S₃ systems which were deployed as counter-electrode in dye-sensitized solar cells (DSSCs).

© 2015 Elsevier B.V. All rights reserved.

1. Introduction

Dye-sensitized solar cells (DSSCs) based on nanocrystalline TiO₂ films have attracted attention in the field of renewable energy owing to their comparatively high solar energy conversion efficiency, easy fabrication procedure and low production cost [1,2]. DSSCs encompasses dye-sensitized nanocrystalline semiconductor electrode (TiO₂), an electrolyte with a redox couple (I₃⁻/I⁻), and a counter electrode, in which I₃⁻ is reduced to I⁻ by the electrons flowing through the external circuit [1–12]. Widespread investigations on the individual components of DSSCs have been performed to produce economical and high performance DSSCs [13–18]. Out of these components the counter electrode (CE) is one of the most crucial components of DSSCs [19]. FTO glass laden with the noble metal platinum is commonly used as the CE, because Pt displays high electrocatalytic activity for I₃⁻ → I⁻ reduction. In view of the scarcity of Pt, other inorganic materials exhibiting efficient electrocatalytic activity in reducing I₃⁻ (e.g., CoS and TiN) have also been used as an alternative catalytic material for the CE [20–22].

Amongst most of the metallic sulfides, bismuth sulfide (Bi₂S₃) is one of the most important V–VI semiconductors, and has attracted great attention for its technological applications. It is a semiconductor having direct band gap (*E_g*) of 1.3 eV [23,24] and has found applications in the field of photovoltaic material, photodiode array, sensor and in IR spectroscopy [25,26]. Also bismuth sulfide belongs to a family of solid-state materials with application in thermometric cooling technology because of the Peltier effect [27]. Significant effort has been made toward the syntheses of Bi₂S₃ nano-particles or their films. Pyrolysis of tris(benzylthiolato)bismuth produced pure Bi₂S₃ polycrystalline [28]. The synthesis of Bi₂S₃ fiber using bismuth dithiocarbamate complexes as single-source precursor by a CVD method [29] and using thermal decomposition in organic solution has also been reported [30–32]. Recently optical and photovoltaic properties of Bi₂S₃ nanorods have been evaluated [33]. In addition to the attempts for the syntheses of pure sulfides of bismuth, a bismuth sulfide-polymer nanocomposite using highly soluble xanthate precursor had been reported [34]. Also, an enhanced photoresponse using Bi₂S₃-Bi₂O₃ has been reported [35]. With these viewpoints and in the quest of new single-source precursors for bismuth and bismuth sulfide, herein we wish to report the synthesis, characterization and the low-cost counter electrode application for a newly synthesized homoleptic

* Corresponding authors. Tel.: +91 9451891030 (A. Kumar).

E-mail addresses: kcm68win@outlook.com (K.C. Molloy), abhinavmarshal@gmail.com (A. Kumar).

[Bi(dtc)₃] (**1**) (dtc = 4-hydroxypiperidine dithiocarbamate) complex as single-source precursor for Bi–Bi₂S₃.

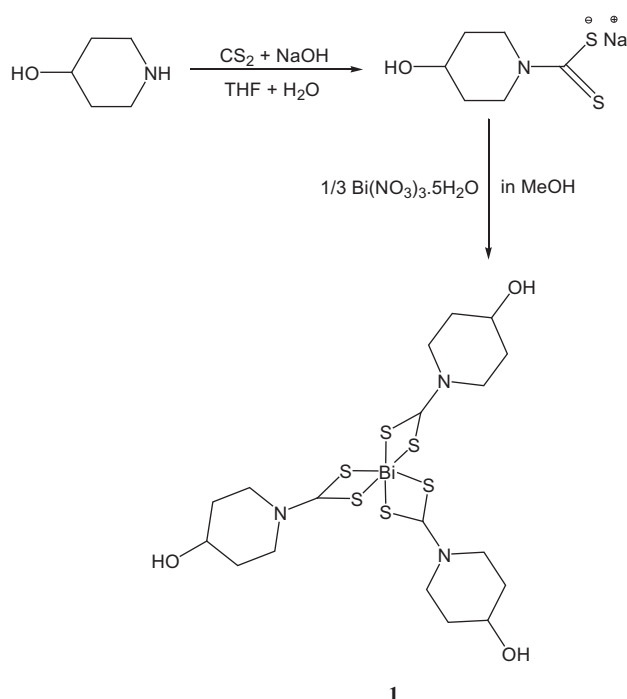
2. Experimental

2.1. Materials and physical measurements

All the synthetic manipulations were performed under ambient atmosphere. The solvents were dried and distilled before use by following the standard procedures. ¹H and ¹³C NMR spectra were recorded on JEOL AL300 FTNMR spectrometer. Chemical shifts were reported in parts per million using TMS as internal standard. The electronic absorption spectra in DMSO solution were recorded using a SPECORD 200 PLUS BU UV–Vis spectrophotometer. Elemental analysis was performed on an Exeter analytical Inc. “Model CE-440 CHN analyser”. Structural characterization of Bi and Bi₂S₃ was done using X-ray diffraction (XRD) measurements on a Bruker D8 Advance X-ray diffractometer equipped with graphite monochromator using Cu Kα (λ = 1.54 Å) radiation, at a scanning rate of 0.21° min⁻¹. The SEM–EDS analyses were carried out using a SIRION FESEM instrument. FESEM images for the samples were carried out by Hitachi S-4800 scanning electron microscopy. TEM analysis were carried out by TEM Techni.

2.2. Synthesis of [Bi(HOCH(CH₂)₄NCS₂)₃] (**1**)

4-hydroxypiperidine (0.303 g, 3 mmol) was dissolved in 15 mL of anhydrous THF and to it was added NaOH (0.120 g, 3 mmol) dissolved in 0.5 mL of water. The mixture was stirred for 10 min and then CS₂ (0.273 g, 3.6 mmol) was added. The mixture was stirred for an additional 30 min until the color of the solution became yellow. To the resulting mixture bismuth nitrate pentahydrate (0.485 g, 1 mmol) dissolved in methanol (10 mL) was added dropwise and the solution was additionally stirred for another 1 h. The resulting solution was filtered and evaporated at room temperature to obtain yellow colored crystals of [Bi(HOCH(CH₂)₄NCS₂)₃].



Scheme 1. Synthesis of the complex **1**.

[Bi(HOCH(CH₂)₄NCS₂)₃] (**1**) (0.582 g, yield 79%); m.p. 241 °C. ¹H NMR (CDCl₃, δ): 5.28 (s, 1H, –OH), 5.24 (s, 2H, –CH), 3.84 (s, 2H, –CH_{ax}), 3.63 (s, 2H, –CH_{eq}), 1.99 (s, 2H, –CH_{ax}), 1.83 (s, 2H, –CH_{eq}), 1.73 (s, 2H, –CH_{ax}). ¹³C NMR (CDCl₃, δ): 199.8 (–NCS₂), 64.8, 47.9, 33.8 (piperidine). ν_{max} (KBr)/cm⁻¹ 3403 (–OH), 1434 (C=N), 1081 (C–S). Anal. Calc. for C₁₈H₃₀N₃O₃S₆Bi: C, 29.30; H, 4.10; N, 5.60; S, 26.08. Found: C, 30.10; H, 4.28; N, 5.74; S, 27.23%.

2.3. X-ray crystallography

Intensity data for **1** was collected at 150(2) K on a Nonius Kappa CCD diffractometer using graphite monochromated Mo Kα radiation λ = 0.71073 Å. Unit cell determination, scaling of the data, and corrections for Lorentz and polarization effects were performed with Denzo-SMN [36]. The structure was solved by direct methods (SIR97) [37] and refined by a full-matrix least-squares procedure based on F² [38]. All non-hydrogen atoms were refined anisotropically; hydrogen atoms were located at calculated positions and refined using a riding model. The asymmetric unit of **1** consists of half a dimeric Bi complex and one solvent molecule of MeOH. One OH-group (O2/O2A) is disordered over two sites in the ratio 60:40. All hetero hydrogen atoms have been located in the difference Fourier map and were refined with bond lengths restraints.

Crystal data: C₃₈H₆₆Bi₂N₆O₈S₁₂, M = 1537.64, triclinic, P $\bar{1}$, a = 8.82520(10) Å, b = 11.5573(2) Å, c = 15.2345(2) Å, α = 102.3288 (9), β = 101.2230(10), γ = 107.6689(7), V = 1389.09(3) Å³, Z = 1, D_{calc} = 1.838 mg m⁻³, F(000) = 758, crystal size 0.25 × 0.20 × 0.05 mm, reflections collected 19089, independent reflections 6319 [R_{int} = 0.0903], final indices [I > 2σ(I)] R₁ = 0.0453 wR₂ = 0.1118, R indices (all data) R₁ = 0.0484, wR₂ = 0.1134, GOF 1.051, largest difference peak and hole 3.004 and –4.330 e Å⁻³.

2.4. Syntheses of Bi₂S₃

2.4.1. Synthesis of **1**

Decomposition of the precursor complex was performed at 550 °C for 6 h in an argon gas atmosphere in a tubular furnace (with a heating rate of 10 °C min⁻¹). The obtained product **1** was washed thrice with de-ionised water (15 mL) and air-dried.

2.4.2. Synthesis of **1a**

In solvothermal decomposition the precursor complex was dissolved in ethylene glycol (15 mL) and heated to 250 °C under argon atmosphere to obtain bismuth sulfide **1a**.

2.4.3. Synthesis of **1b**

In a capping agent mediated synthesis the precursor (0.200 g) was added to ODA (*n*-octadecylamine, 2.330 g) at 75 °C under nitrogen atmosphere. The reaction mixture was heated up to 200 °C with mild stirring for 3 h. After 3 h, it was cooled to 90 °C and then ethanol (50 mL) and toluene (15 mL) solvent mixture was added. The solid powder **1b** was isolated after centrifugation followed by drying under vacuum.

2.4.4. Synthesis of **1c**

The precursor (0.200 g) was added to DDT (dodecanethiol, 2.14 mL) at room temperature under nitrogen atmosphere. Then the reaction mixture was heated at 160–170 °C with gentle stirring for 3 h. The precursor started decomposing at lower temperature in presence of the capping agent as compared to solid state. At the end of decomposition the solid product was washed with ethanol (4 × 25 mL) followed by washing with diethyl ether (30 mL) and finally centrifuged to collect **1c** which was dried under vacuum.

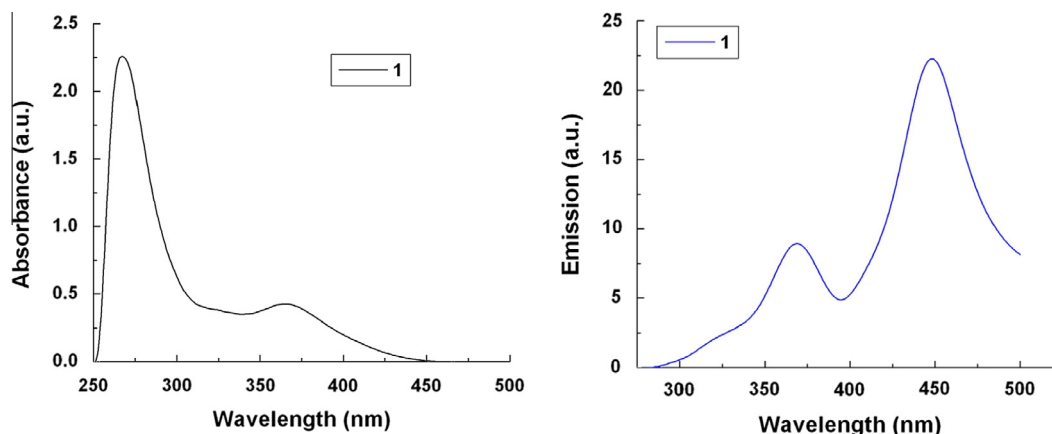


Fig. 1. Electronic absorption (left) and normalized photoluminescence (right) spectra of the complex in 10^{-3} M DMSO solution.

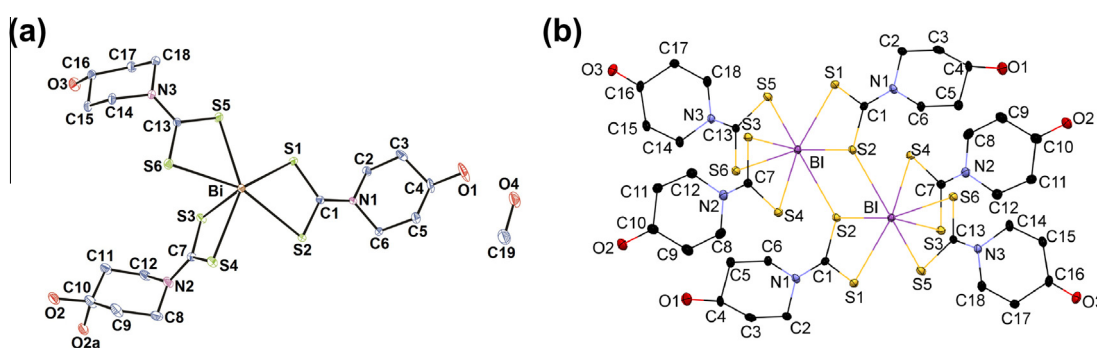


Fig. 2. Perspective view of (a) molecular structure of **1**; (b) the dimer held by Bi...S interactions. Hydrogen atoms have been omitted for clarity.

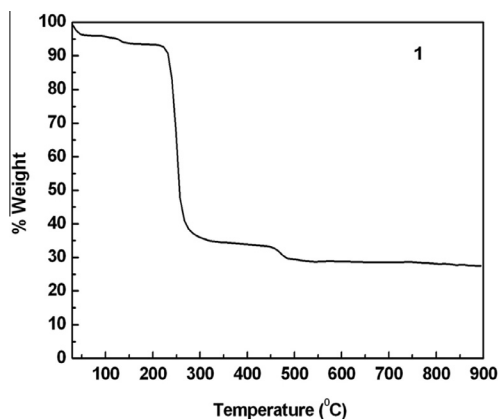


Fig. 3. TGA curve for the complex **1**.

2.5. DSSC fabrication

Transparent conductive glass plates coated with an F-doped SnO_2 (FTO, purchased from Pilkington. Co., Ltd., $8 \Omega/\gamma$) were used to prepare both the photo- and counter-electrodes. Approximately 0.05 g of Bi_2S_3 powder was mixed with 0.5 ml 2.5% PEG20000 solution and stirred until a fluid mixture formed. A film was then made using the doctor-blade method on FTO conductive glass. The film was heated at 450°C for 1 h under the protection of argon to obtain the Bi_2S_3 counter electrode. Commercialized TiO_2 paste (Ti-Nanoxide T, Solaronix) was casted onto the heat-treated FTO substrates by the doctor-blade technique and then sintered at 450°C for 30 min. The substrates with

thick mesoporous TiO_2 layers (ca. 13–18 μm) and the film was soaked in an N-719 dye solution (in ethanol) for 24 h to obtain dye-sensitized TiO_2 electrodes. The unadsorbed dye was washed out with anhydrous ethanol. The dye-adsorbed TiO_2 electrodes and Bi_2S_3 counter-electrodes were assembled into a sealed sandwich-type cell by heating at 80°C using a hot-melt ionomer film (Surlyn) as a spacer between the electrodes. The electrolyte was composed of 0.6 M 3-hexyl-1,2-dimethylimidazolium iodide, 0.05 M iodine, 0.05 M LiI and 0.5 M 4-tert. butyrypyridine in acetonitrile. A drop of electrolyte solution was placed in a hole drilled in

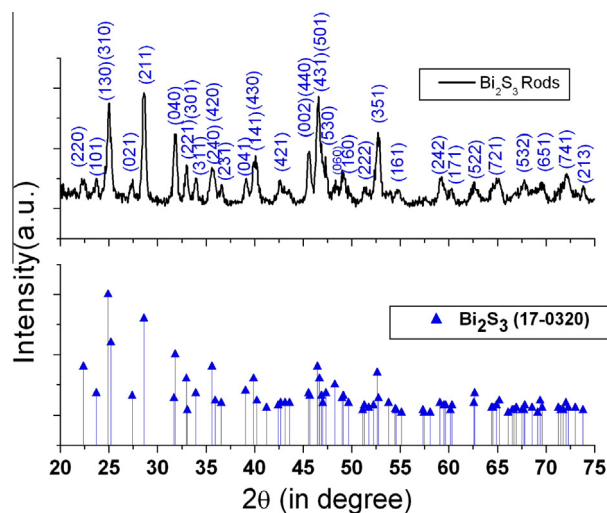


Fig. 4. Powder X-ray diffractograms of decomposed product of **1a** obtained solvothermally without capping agent.

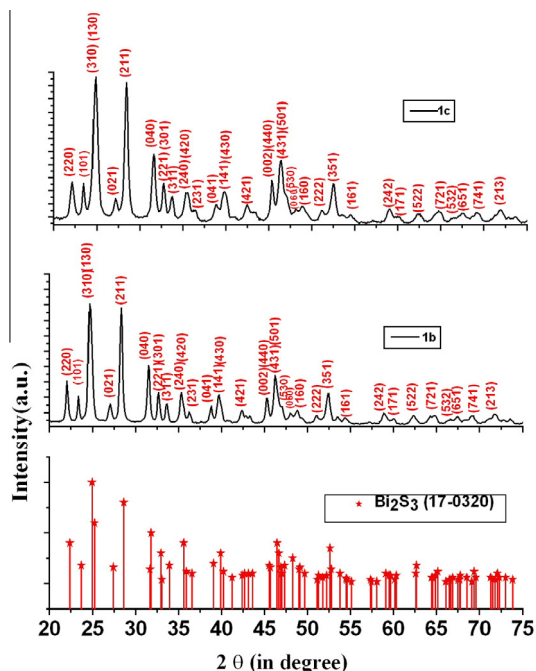


Fig. 5. Powder X-ray diffractograms of decomposed product of **1b** and **1c** obtained solvothermally using capping agents.

the counter-electrode and driven into the cell *via* vacuum backfilling. Finally the hole was sealed using additional Surllyn and a 0.1 mm thick glass cover.

2.6. Solar cell efficiency

The photoelectrochemical performance characteristics (short circuit current J_{sc} (mA cm^{-2}), open-circuit voltage V_{oc} (V), fill factor ff and overall conversion efficiency η) were measured under illumination with a 1000 W xenon lamp (Oriol 91193) using a Kiethley Model 2400. The light intensity was confirmed to be homogenous over an $8 \times 8 \text{ in}^2$ area by calibration with a Si solar cell for 1 sun light intensity (AM 1.5G , 100 mW cm^{-2}). Accidental increase in the temperature inside the cell was prevented by using a cooler with a propeller.

2.7. Electrochemical impedance spectroscopy

The electrochemical impedance spectroscopy (EIS) was performed on a CH 660C electrochemical analyzer (CH Instruments, Shanghai, China) in a two electrode configuration. The photoanode was used as a working electrode and the Pt electrode as a counter electrode. The electron transport properties were investigated using electrochemical impedance spectroscopy (EIS) with 10 mV alternative signal in the frequency range of 10^{-2} to 10^5 Hz .

3. Results and discussion

3.1. Synthesis

The complex $[(\text{HOCH}(\text{CH}_2)_4\text{NCS}_2)_3\text{Bi}]$ (**1**) was obtained by the addition of stoichiometric amounts of metal salt and sodium 4-piperidinoldithiocarbamate in a mixture of THF, water and methanol (Scheme 1). The complex **1** was air stable and moderately soluble in water, acetone, methanol, acetonitrile, DMSO and DMF but insoluble in halogenated solvents. Crystals of **1** suitable

for X-ray structural analysis were obtained by slow evaporation of a methanol/water mixture.

3.2. Spectroscopy

The purity and composition of the complex was checked by ^1H NMR spectroscopy. All the ^1H NMR signals correspond to the piperidine moiety of the dithiocarbamate ligand. In ^{13}C NMR the signal at $\sim 199 \text{ ppm}$ corresponds to the thioureide (NCS_2) function.

The IR spectrum of complex **1** shows a distinct vibrational band at around $\sim 1100 \text{ cm}^{-1}$ which is associated with the symmetric bidentate $\nu(\text{CS}_2)$ vibration of the dithiocarbamate ligand. The band near 1435 cm^{-1} is characteristic of the thioureide vibration and is associated with the $\nu(\text{C-N})$ which is appreciably higher than the free ligand and thereby indicates significant increase in the partial double bond character of C–N bond. Additionally, the band at $\sim 3435 \text{ cm}^{-1}$ is indicative of the free –OH function in the piperidino moiety.

The electronic absorption spectrum for **1** was recorded in DMSO (Fig. 1). The bands observed below 275–400 nm are mainly the ligand centered displaying $\pi \rightarrow \pi^*$ and intraligand charge transfer transition behavior [39,40]. When excited at 275 nm the compound displays broad emissions at $\sim 360 \text{ nm}$ and 450 which arise from the intraligand charge transfer (Fig. 1) [39].

3.3. Molecular structure description

The molecular structure of complex **1** with atomic numbering scheme is shown in Fig. 2(a). Complex **1** crystallizes in the triclinic crystal system with space group $P\bar{1}$. The asymmetric unit of **1** contains half a dimeric bismuth complex, one solvent molecule of MeOH; one OH-group (O2/O2A) is disordered over two sites in the ratio 60:40. The central bismuth is six-coordinate by six sulfur atoms belonging to three 4-hydroxypiperidine ligands. The resulting Bi_6 coordination polyhedron approximates a pentagonal pyramid with atoms Bi and S1–S6 at the base of the pyramid and S3 in the apical position. The five equatorial Bi–S bonds are long [S1–S2 to S4–S6; mean = $2.838(13) \text{ \AA}$] while the apical donor atom forms the strongest bond [Bi–S3 = $2.6225(12) \text{ \AA}$]. The Bi^{III} lone pair of electrons may project in a direction roughly trans to the Bi–S3 bond. In complex **1**, Bi^{III} adopts a distorted pentagonal-pyramid, due to its stereochemically active lone pair of electrons. A long $\text{Bi} \cdots \text{S}$ [Bi–S(2')] contact of $3.2393(13) \text{ \AA}$ leads to dimeric associations of molecules in the crystal structure as shown in Fig. 2(b). Within the dithiocarbamate function, C–N_{dtc} bond lengths of 1.325 – 1.346 \AA indicate a substantial delocalization of the π -electron density in this bond [41]. The six membered 4-hydroxy piperidine ring adopts the chair conformation.

3.4. Thermal properties

Thermal decomposition of complex **1** was performed under nitrogen atmosphere (Fig. 3). The TGA profile displays two-step decomposition with a third small weight loss (*ca.* 7%) in the outset, which can be attributed to the escape of methanol from the system. The first major weight loss (*ca.* 60%) was observed around $260 \text{ }^\circ\text{C}$ whereas the smaller second weight loss (*ca.* 6%) was found to occur around $470 \text{ }^\circ\text{C}$. The total weight loss led to the residual Bi and all the other components decomposed to different gases and other volatile compounds.

3.5. pXRD and SEM

The pXRD of the decomposed product of **1** obtained by heating under argon atmosphere at $550 \text{ }^\circ\text{C}$ for 6 h is presented in Fig. S1

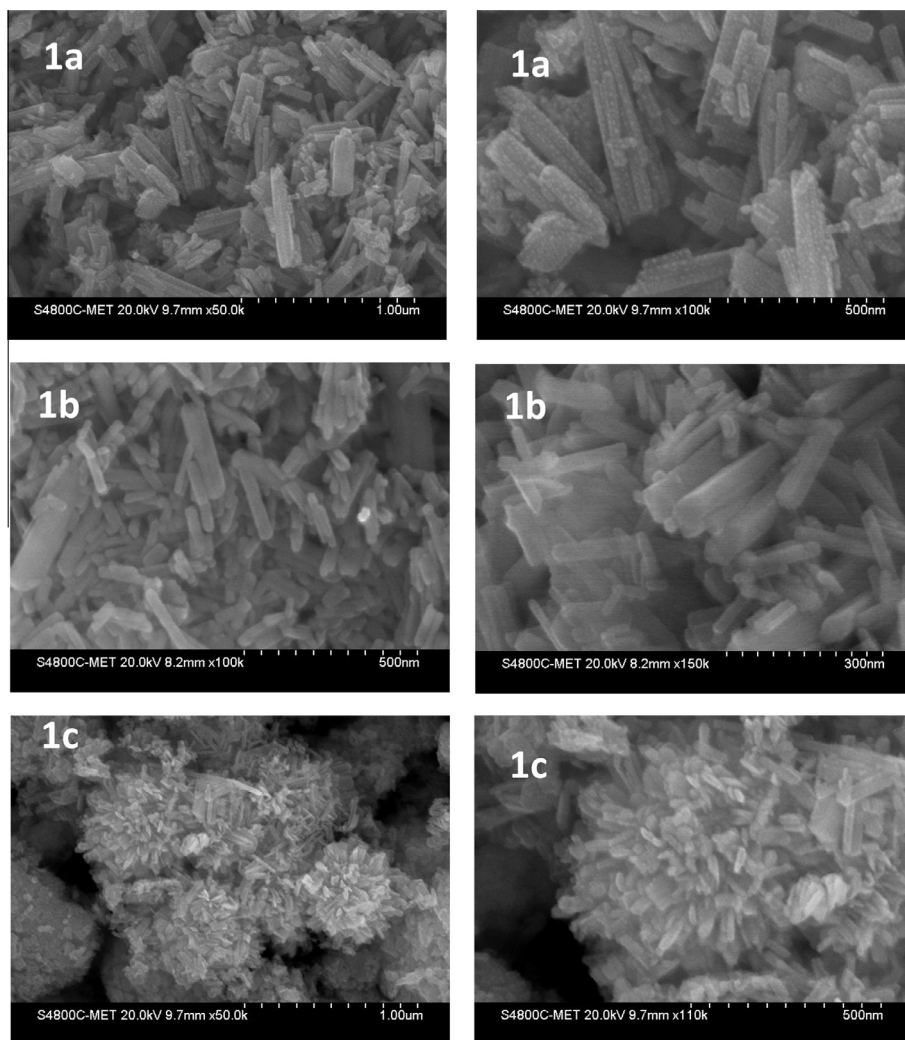


Fig. 6. SEM micrographs of **1a**, **1b** and **1c** at different magnifications.

(Supplementary informations). The indexed data matches with the pure bismuth (JCPDS No. 05-0519) and bismuth sulfide Bi_2S_3 (JCPDS No. 06-0333). Hence, from the pXRD data it is clearly evident that the obtained decomposed product is a mixture of $\text{Bi-Bi}_2\text{S}_3$.

In order to have an idea regarding the relative composition of the mixture, EDAX analysis was performed which indicated that the amount of bismuth is more in comparison to Bi_2S_3 . The composition from EDAX is $\text{Bi}_{9.77}\text{S}_{3.03}$ which means that it is approximately $7\text{Bi}:\text{Bi}_2\text{S}_3$.

SEM micrographs for the decomposed product obtained from **1** indicated the formation of agglomerated rods (Fig. S2 Supplementary informations).

Solvothermal decomposition of **1** in both the absence (**1a**) and presence of two different capping agents **1b**, **1c** (see Section 2) led to the formation of pure Bi_2S_3 and the characteristic pXRDs are presented in Figs. 4 and 5. The indexed data matches with the pure bismuth sulfide Bi_2S_3 (JCPDS No. 17-0320) in all the three cases. The FESEM images for all the three Bi_2S_3 systems indicate the formation of aggregated rods. However, in these capping agent-assisted syntheses the dimensions of the rods are relatively smaller. The nanorods in case of **1a** are 400–600 nm in length and 20–30 nm in diameter, nanorods in **1b** are 200–300 nm in length and 20–25 nm in diameter whereas nanorods in **1c** shows length 100–150 nm long and 10–20 nm in diameter, which exhibiting larger surface area for greater catalytic activity and hence possess

relatively larger specific surface area than those from the bulk decomposition (Fig. 6). This larger surface area may impose better cell performance of DSSCs when these sulfides are employed as the counter electrode.

The TEM images for **1a**, **1b** and **1c** are shown in Fig. 7. The fringes spacing of 0.230 nm for **1a** and 0.199 nm for **1b**, **1c** in concur with the spacings of the (002) and (120) lattice planes of orthorhombic Bi_2S_3 , respectively, signifying that the exposed (211) facet for **1a** and (130) facets for **1b** and **1c** are upright to (120) and (002) planes, respectively.

4. Counter electrode applications

The obtained Bi_2S_3 products with different morphologies were tested as counter electrodes in dye-sensitized solar cells (DSSCs) using N-719 dye. The current potential curves using different Bi_2S_3 (**1a–1c**) as counter electrodes are presented in Fig. 8. The relevant photovoltaic parameters are presented in Table 1. As evident from data presented, the performance of Bi_2S_3 **1c** is relatively better than **1a** and **1b**. In fact, the cell performance increases monotonically with decrease in size of the Bi_2S_3 rods. This better performance may be attributed to the relatively larger specific surface area of **1c** than either **1a** or **1b**. Still, the conversion efficiencies remain lower than the conventional platinum counter electrode showing efficiency of 6.4% [42]. Also, carbon black/ TiO_2 composites

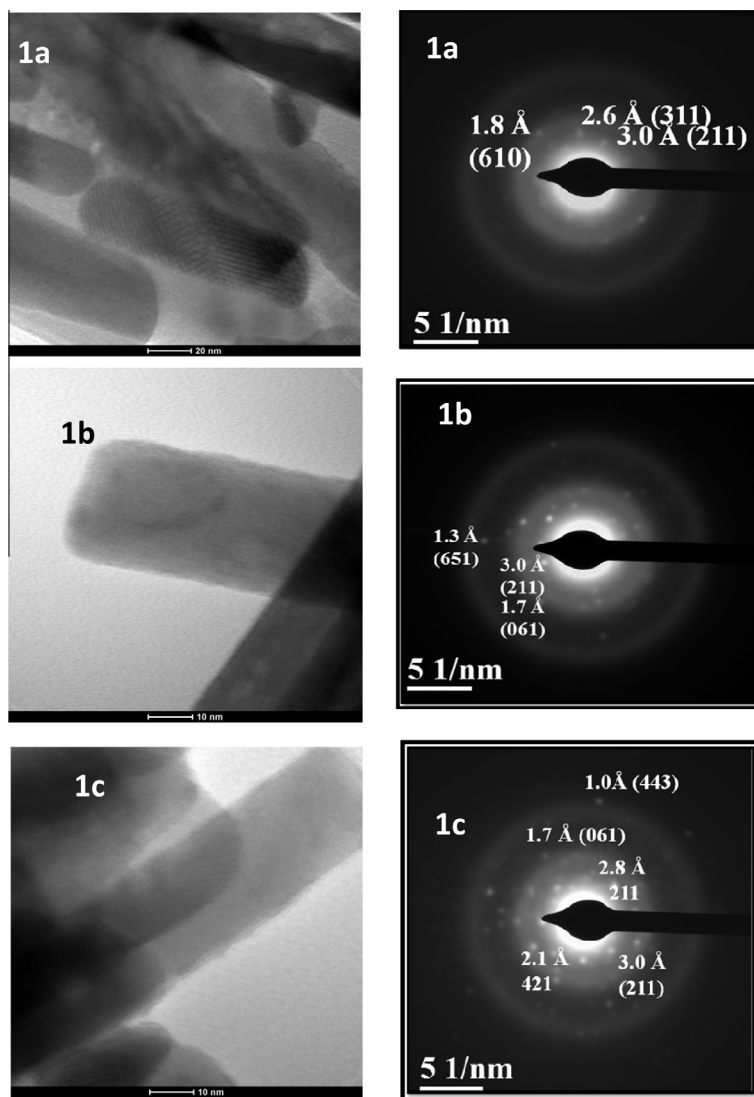


Fig. 7. TEM and SAED patterns for **1a**, **1b** and **1c**.

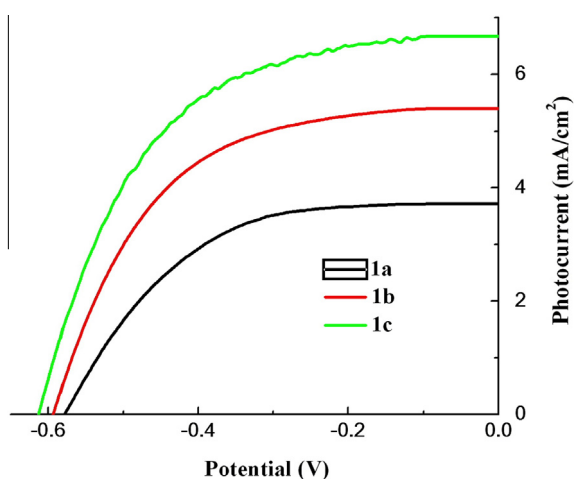


Fig. 8. IV curve obtained for different Bi_2S_3 counter electrodes.

have led to very close efficiency of 5.5% [42]. But, by engineering the grain sizes [43], and also by preparing the graphene composites [44,45] of the synthesized Bi_2S_3 , the cell performance can be improved. Hence Bi_2S_3 can become a low cost alternative to the conventional but costly Pt counter electrode for DSSCs.

Electrochemical impedance spectroscopy (EIS) was employed to study the electron recombination and electrolyte reduction process in DSSCs. Fig. 9 shows the alternating-current impedance spectra of the DSSCs measured under illumination. The semicircle in the high-frequency range corresponds to charge transfer behavior at the counter electrode/electrolyte interface. The smaller radius of semicircle indicates lower impedance, and thus better electrical conductivity. According to semicircle radius the electrical

Table 1
The photovoltaic parameters for the different Bi_2S_3 counter electrodes.

	J_{sc} (mA cm^{-2})	V_{oc} (V)	FF	η (%)
1a	3.72	-0.578	0.52	1.11
1b	5.40	-0.590	0.56	1.79
1c	6.67	-0.612	0.55	2.25

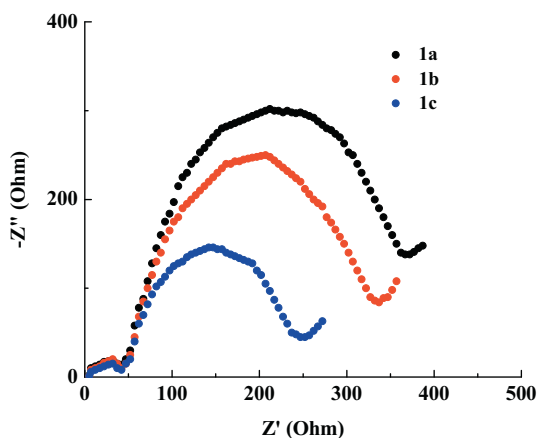


Fig. 9. Nyquist plots of DSSCs based on the **1a**, **1b** and **1c** counter electrodes.

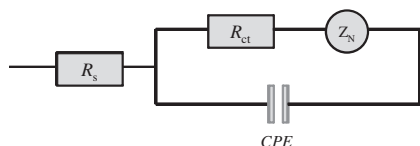


Fig. 10. Circuit diagram for **1a**, **1b** and **1c** used as the counter electrode.

conductivity decreases in the order of **1c** > **1b** > **1a**. Zhang et al. explained about the facet dependent performance of Bi_2S_3 counter electrode that (130) facet has shown better performance than (211) facet due to larger surface energy of (130) facet of Bi_2S_3 [43]. This facet concept of Zhang et al. is in good agreement with our result, **1b** and **1c** has (130) facets shown better cell performance than **1a** (211).

The circuit diagram for **1a**, **1b** and **1c** used as counter electrode is presented in Fig. 10. The power conversion efficiency depends on the internal resistance of the system, which mainly composed of series resistance (R_s) and charge transfer resistance (R_{ct}) [46,47]. The series resistance (R_s) is due to bulk resistance of catalytic materials, resistance of FTO glass substrate, and contact resistance while the R_{ct} represents the catalytic properties of the electrode for reducing triiodide ion. A constant phase element (CPE) describing deviation from the ideal capacitance and charge transfer resistance R_{ct} corresponds to the first semicircle (mid-frequency: 100–0.1 kHz). The low-frequency (around 100 Hz) region represents the Nernst diffusion impedance (Z_N) of the redox couple in the electrolyte. The R_{ct} values in decreasing order for the systems are **1a** > **1b** > **1c** is probably due to the larger catalytic active surface area.

5. Conclusions

Based on the findings of the present investigation it can be concluded that the synthesized $\text{Bi}(\text{dtc})_3$ complex can be a potential single-source precursor for Bi_2S_3 . By varying the nature of capping agents the solvothermal decomposition can yield Bi_2S_3 of different morphologies and sizes having relatively larger specific surface area which can be employed as counter electrode in DSSCs.

Acknowledgements

AK and RC are grateful to Department of Science and Technology, New Delhi and INSA for financial support in the form of project SB/FT/CS-018/2012 and IFA12-CH-34, respectively.

Appendix A. Supplementary material

CCDC 1034636 contains the supplementary crystallographic data for complexes. These data can be obtained free of charge from The Cambridge Crystallographic Data Centre via www.ccdc.cam.ac.uk/data_request/cif. Supplementary data associated with this article can be found, in the online version, at <http://dx.doi.org/10.1016/j.ica.2015.03.007>.

References

- [1] B. O'Regan, M. Grätzel, *Nature* 353 (1991) 737.
- [2] M. Grätzel, *Nature* 414 (2001) 338.
- [3] A. Hagfeldt, G. Boschloo, L.C. Sun, L. Kloo, H. Pettersson, *Chem. Rev.* 110 (2010) 6595.
- [4] M. Grätzel, *Acc. Chem. Res.* 42 (2009) 1788.
- [5] S. Ardo, G.J. Meyer, *Chem. Soc. Rev.* 38 (2009) 115.
- [6] K. Kalyansundaram, *Photochemical and Photoelectrochemical Approaches to Energy Conversion*, EPFL Press, 2010.
- [7] F. De Angelis, in: K. Kalyansundaram (Ed.), *Dye Sensitized Solar Cells*, EPFL Press, Swiss Academic Publisher, 2010.
- [8] A. Kumar, R. Chauhan, K.C. Molloy, G. Kociok-Köhn, L. Bahadur, N. Singh, *Chem. Eur. J.* 16 (2010) 4307.
- [9] R. Chauhan, M. Trivedi, L. Bahadur, A. Kumar, *Chem. Asian J.* 6 (2011) 1525.
- [10] R. Chauhan, S. Auvinen, A.S. Aditya, M. Trivedi, R. Prasad, M. Alatalo, D.P. Amalnerkar, A. Kumar, *Sol. Energy* 108 (2014) 560.
- [11] A. Kumar, S. Auvinen, M. Trivedi, R. Chauhan, M. Alatalo, *Spectrochim. Acta A* 115 (2013) 106.
- [12] J.H. Wu, S.C. Hao, Z. Lan, J.M. Lin, M.L. Huang, Y.F. Huang, P.J. Li, T. Sato, *J. Am. Chem. Soc.* 130 (2008) 11568.
- [13] M.K. Nazeeruddin, F.D. Angelis, S. Fantacci, A. Selloni, G. Viscardi, P. Liska, S. Ito, B. Takeru, M. Grätzel, *J. Am. Chem. Soc.* 127 (2005) 16835.
- [14] H. Choi, I. Raabe, D. Kim, F. Teocoli, C. Kim, K. Song, J.H. Yum, J. Ko, M.K. Nazeeruddin, M. Grätzel, *Chem. Eur. J.* 16 (2010) 1193.
- [15] Y. Luo, D. Li, Q. Meng, *Adv. Mater.* 21 (2009) 4647.
- [16] S. Yanagida, Y. Yu, K. Manseki, *Acc. Chem. Res.* 42 (2009) 1827.
- [17] H. Choi, S.O. Kang, J. Ko, G. Gao, H.S. Kang, M.S. Kang, M.D. Nazeeruddin, M. Grätzel, *Angew. Chem., Int. Ed.* 48 (2009) 5938.
- [18] H. Choi, C. Baik, S.O. Kang, J. Ko, M.S. Kang, M.D. Nazeeruddin, M. Grätzel, *Angew. Chem., Int. Ed.* 47 (2008) 327.
- [19] T.N. Murakami, M. Grätzel, *Inorg. Chim. Acta* 361 (2008) 572.
- [20] M.K. Wang, A.M. Anghel, B. Marsan, N.C. Ha, N. Pootrakulchote, S.M. Zakeeruddin, M. Grätzel, *J. Am. Chem. Soc.* 131 (2009) 15976.
- [21] Q.W. Jiang, G.R. Li, X.P. Gao, *Chem. Commun.* (2009) 6720.
- [22] G.R. Li, F. Wang, Q.W. Jiang, X.P. Gao, P.W. Shen, *Angew. Chem., Int. Ed.* 49 (2010) 3653.
- [23] J.D. Klein, R.D. Herrick, D. Palmer, M.J. Sailor, *Chem. Mater.* 5 (1993) 902.
- [24] M. Aresti, M. Saba, R. Piras, D. Marongiu, G. Mula, F. Quochi, A. Mura, C. Cannas, M. Mureddu, A. Ardu, G. Ennas, V. Calzia, A. Mattoni, A. Musinu, G. Bongiovanni, *Adv. Funct. Mater.* 24 (2014) 3341.
- [25] C.R. Martin, *Science* 266 (1994) 1961.
- [26] D. Routkevitch, T. Bigioni, M. Moskovits, J.M. Xu, *J. Phys. Chem.* 100 (1995) 14037.
- [27] P. Boudjouk, D.G. Grier, B.R. Jarabek, G.J. McCarthy, *Inorg. Chem.* 37 (1998) 3538.
- [28] O.C. Monteiro, T. Trindade, J.H. Park, P. O'Brien, *Chem. Vap. Dep.* 6 (2000) 230.
- [29] O.C. Monteiro, T. Trindade, *Mater. Sci. Lett.* 19 (2000) 859.
- [30] O.C. Monteiro, H.I.S. Nogueira, T. Trindade, *Chem. Mater.* 13 (2001) 2103.
- [31] S.S. Warule, N.S. Chaudhari, B.B. Kale, S. Pandiraj, R.T. Khare, M.A. More, *CrystEngComm* 15 (2013) 890.
- [32] Y.W. Koh, C.S. Lai, A.N. Du, E.R.T. Tiekink, K.P. Loh, *Chem. Mater.* 15 (2003) 4544.
- [33] H.-C. Liao, M.-C. Wu, M.-H. Jao, C.-M. Chuang, Y.-F. Chen, W.-F. Su, *CrystEngComm* 14 (2012) 3645.
- [34] V. Kaltenhauser, T. Rath, W. Haas, A. Torvisco, S.K. Müller, B. Friedel, B. Kunert, R. Saf, F. Hofer, G. Trimmel, *J. Mater. Chem. C* 1 (2013) 7825.
- [35] F. Lu, R. Li, N. Huo, J. Yang, C. Fan, X. Wang, S. Yang, J. Li, *RSC Adv.* 4 (2014) 5666.
- [36] DENZO-SCALEPACK Z. Otwinowski and W. Minor, "Processing of X-ray Diffraction Data Collected in Oscillation Mode", *Methods in Enzymology*, Volume 276: Macromolecular Crystallography, part A, p. 307–326, 1997, C.W. Carter, Jr. & R. M. Sweet, Eds., Academic Press.
- [37] sr97, A. Altomare, M.C. Burla, M. Camalli, G.L. Casciarano, C. Giacovazzo, A. Guagliardi, A.G.G. Moliterni, G. Polidori, R. Spagna, *J. Appl. Crystallogr.* 32 (1999) 115.
- [38] G.M. Sheldrick, *Acta Crystallogr., Sect. A* 64 (2008) 112.
- [39] S.P. Kaiwar, A. Vodacek, N.V. Blough, R.S. Pilato, *J. Am. Chem. Soc.* 119 (1997) 3311.
- [40] E.G. Bakalbassis, G.A. Katsoulos, C.A. Tsipis, *Inorg. Chem.* 26 (1987) 3151.
- [41] K.A. Wheeler, B. Harrington, M. Zapp, E. Casey, *CrystEngComm* 5 (2003) 337.

- [42] P. Joshi, Y. Xie, M. Ropp, D. Galipeau, S. Bailey, Q. Qiao, *Energy Environ. Sci.* 2 (2009) 426.
- [43] H. Zhang, L. Yang, Z. Liu, M. Ge, Z. Zhou, W. Chen, Q. Lid, L. Liu, *J. Mater. Chem.* 22 (2012) 18572.
- [44] S.-Q. Guo, T.-S. Jing, X. Zhang, X.-B. Yang, Z.-H. Yuan, F.-S. Hu, *Nanoscale* 6 (2014) 14433.
- [45] X.-Q. Zuo, X. Yang, L. Zhou, B. Yang, G. Li, H.-B. Tang, H.-J. Zhang, M.-Z. Wu, Y.-Q. Ma, S.-W. Jin, *RSC Adv.* 4 (2014) 57412.
- [46] Q. Wang, J.E. Moser, M. Grätzel, *J. Phys. Chem. B* 109 (2005) 14945.
- [47] A. Hauch, *Electrochim. Acta* 46 (2001) 3457.